Final Completion Report :

LDMS: A Low-Dimensional Modeling System for Hillslope, Catchment and River-Basin Runoff

by

Christopher J. Duffy
David Brandes
Tong-Ying Shun
Karsten Sedmera

Pennsylvania State University

Submitted 28 February 2000

U.S. Army Research Office

Grant: DAAH04-96-1-0035

Approved for Public Release

Distribution Unlimited

20000628 021

The views, opinions, and/or findings contained in this report are those of the authors and should not be construed as an official Department of the Army position, policy or decision, unless so designated by other documentation.

DTIC QUALITY INSPECTED 4

SF 298 MASTER COPY KEEP THIS COPY FOR REPRODUCTION PURPOSES

REPORT DOCUMENTATION PAGE

Form Approved
OMB NO. 0704-0188

Public reporting burden for this collection of information is estimated to average 1 hour per response, including the time for reviewing instructions, searching existing data sources, gathering and maintaining the data needed, and completing and reviewing the collection of information. Send comment regarding this burden estimates or any other aspect of this collection of information, including suggestions for reducing this burden, to Washington Headquarters Services, Directorate for information Operations and Reports, 1215 Jefferson Davis Highway, Suite 1204, Arlington, VA 22202-4302, and to the Office of Management and Budget, Paperwork Reduction Project (0704-0188), Washington, DC 20503.

1. AGENCY USE ONLY *(Leave blank)*	2. REPORT DATE	3. REPORT TYPE AND DATES COVERED
	28 February 2000	10 April 1996 to 31 December 1999

4. TITLE AND SUBTITLE

LDMS: a Low-Dimensional Modeling System for Hillslope, Catchment and River-Basin Runoff

5. FUNDING NUMBERS

DAAH04-96-1-0035

6. AUTHOR(S)

Christopher Duffy
212 Sackett Building
Civil & Environmental Engineering Department

7. PERFORMING ORGANIZATION NAMES(S) AND ADDRESS(ES)

The Pennsylvania State University
Environmental Resources Research Institute
Land & Water Building
University Park, PA 16802

8. PERFORMING ORGANIZATION REPORT NUMBER

9. SPONSORING / MONITORING AGENCY NAME(S) AND ADDRESS(ES)

U.S. Army Research Office
P.O. Box 12211
Research Triangle Park, NC 27709-2211

10. SPONSORING / MONITORING AGENCY REPORT NUMBER

11. SUPPLEMENTARY NOTES

The views, opinions and/or findings contained in this report are those of the author(s) and should not be construed as an official Department of the Army position, policy or decision, unless so designated by other documentation.

12a. DISTRIBUTION / AVAILABILITY STATEMENT

Approved for public release; distribution unlimited.

12 b. DISTRIBUTION CODE

13. ABSTRACT *(Maximum 200 words)*

In this research we have developed a strategy for dynamical modeling of multi-scale hydrologic systems. The approach assumes that soil moisture and saturated groundwater storage serve as essential state variables in the rainfall-runoff process and that natural variations in topography, drainage area, and depth of moisture penetration serve to define the particular flow geometry. The state variables are formed by "weighted averaging", where the weighting is a conditional probability for terrain features (altitude, aspect and depth of moisture penetration) determined from digital terrain data and a GIS. Similarly, "volume weighted" storage-flux relations are determined. The strategy of "terrain averaging" is proposed here to simplify the model dynamics, retain essential nonlinearity while preserving the local space-time scale (Duffy, 1996). In large regions, however, runoff represents an unknown number of space-time scales, and the question becomes: What is the dimension and complexity of this extended dynamical system? To this end we apply the signal processing technique of Multichannel Singular Spectrum Analysis (MSSA), a generalization of Principal Components Analysis for space-time processes. From multiple precipitation and streamflow time series across the drainage basin, we estimate the time scales of the response and the complexity of our dynamic syste

14. SUBJECT TERMS

Hydrologic dynamical system, nonlinearity, soil moisture, groundwater, runoff, topography

15. NUMBER IF PAGES

16. PRICE CODE

17. SECURITY CLASSIFICATION OR REPORT	18. SECURITY CLASSIFICATION OF THIS PAGE	19. SECURITY CLASSIFICATION OF ABSTRACT	20. LIMITATION OF ABST
UNCLASSIFIED	UNCLASSIFIED	UNCLASSIFIED	UL

Overview and Research Summary

Introduction

This research, funded by a grant from the Army Research Office of Terrestrial Science Hydrology/Geomorpholgy Program, is developing a physically-based, **L**ow-**D**imensional **M**odeling **S**ystem (**LDMS**) for runoff for regions of complex terrain. A traditional approach to rainfall-runoff focuses on channel and surface flow processes. However, this study emphasizes the longer time scales of soil moisture and subsurface storage in controlling runoff, within regions of complex topography and geology. For a single stream-reach, our modeling strategy identifies how hillslope soil moisture and subsurface storage interact with channel processes through direct coupling and feedback from baseflow and bank storage, deep recharge, and saturation-overland flow processes. The model includes the essential components of atmospheric forcing from rainfall, evaporation, transpiration, snow accumulation and snowmelt and their dynamic interaction with soil moisture and saturated groundwater to produce runoff. In the case of stream networks and/or vertically stratified geology contributing to runoff, the hillslope-stream-reach becomes an element in an extended dynamical system. The extended dynamical system is a spatially distributed model which attempts to preserve the statistically important time/space scales of the catchment runoff. In this sense, a particular hillslope and corresponding stream-reach represents a spatial random variate (Duffy, 1996) from the underlying distribution of hillslopes within the watershed or drainage basin. At any point within the stream network, runoff represents an integration of the upland contribution from spatially random elements of hillslope storage and flux. From this perspective, the question for prediction is: What is the distribution of contributing hillslopes and what are their "expected" time/space scales? From our signal processing and dimension estimation work, the number of time scales contributing to runoff seems to be limited, with only a few hillslope scales contributing most of the runoff. The number of states contributing to runoff becomes a problem of state-space dimension estimation.

This report will outline a systematic approach to the problem of physically-based modeling in complex terrain involving four basic steps:

- Dynamical model development at the hillslope-stream-reach scale.
- State-space dimension estimation from historical streamflow and hydroclimatic observations.
- Conceptual-mathematical model development based on terrain features, geology and the relation to the stream network.
- Model and parameter identification/calibration and verification

The first phase of this research effort has involved the development of a hillslope dynamical modeling system which couples the dynamics (feedback and interaction) of the important physical processes within a stream reach. A paper by Duffy (1996) and a dissertation by Lee (1994) provides details of the first development of the model. Recent progress has involved examining the stability of the hillslope-stream-reach system, and an extension of the model to include the effects of macroporous soils and rocks on soil moisture, groundwater storage and runoff timing. A paper on the stability of the hillslope component of the model was recently published (Brandes, Duffy and Cusumano, 1998), and another paper has been completed on the macropore extension of the model Brandes and Duffy, 2000).

The problem of dimension estimation and the forming of the hydrogeologic conceptual model is an essential ingredient in the LDMS approach. Qualitatively, the characteristic terrain of physiographic regions of North America implies some measure of similarity in form. Hydrologists have also known that there seem to be a limited set of time/space scales contributing to runoff (Jakeman and Hornberger, 1984). Here we attempt to move beyond this qualitative notion of "characteristic terrain", to a quantitative statistical method to estimate the dimension of the state-space contributing to runoff at a point. It can be thought of as the number of independent hillslopes (time/space scales), which make up the dominant contribution to the runoff time series. We have adopted the signal processing technique of singular spectrum analysis, also known as Karhunen-Loeve decomposition or principal orthogonal decomposition as a means of estimating this dimension from historical precipitation-temperature runoff data. We have applied the approach to mountain-front runoff response for the Wasatch Front (Shun and Duffy, 1998), the Susquehanna, Rio Grande, Colorado and Washita rivers in the US. The dimension estimation amounts to a partitioning of time variance of runoff into independent components. A ranking of the eigenvalues for each independent component gives a measure of the relative contribution of each independent mode (eigenvector) to the overall runoff signal. The dominant modes of fluctuation are then qualitatively related to characteristic terrain features , soils and geology. This leads to a conceptual model of the hydrology-hydrogeology, the hillslope-stream-reach dynamcial model and finally to an estimate of the extended dynamical system for watershed.

The final phase of the research is the development of a calibration and validation procedure with field applications over a range of physiographic, climatic and geologic conditions across North America. We have successfully incorporated an optimization algorithm based on the genetic algorithm. The genetic algorithm serves two purposes:

- The algorithm performs a random search of the expected range of the physical parameter space and allows the user to utilize available hydraulic and physiographic information on the soil and geologic material (e.g. porosity, hydraulic conductivity), terrain features (slope, length of flow, contributing area) from the watershed database.

- It allows the modeler to test the relative significance of adding new state variables (hillslope-reach, or deeper geologic strata) to improve the model performance.

The case study presented here is the Upper West Branch of the Susquehanna River. This paper has recently been submitted to Water Resources Research (Shun and Duffy, 2000). A second model application is underway in the Washita River basin in Oklahoma and this paper is in progress. The third application is the Shale Hills watershed near State College, PA. The model has been implemented, parameters estimated and a paper will be completed during 2000.

The Dynamical Hillslope-Stream-Reach Model

A dynamical model is devised for a where unsaturated and saturated storage serve as the principal control on rainfall-runoff, and where complex topography, drainage area and variable depth of moisture penetration describe the flow geometry. The model is formed by direct integration of the local conservation equation with respect to the partial volumes occupied by unsaturated and saturated moisture storage, respectively (Duffy, 1996). This yields an "integral-balance" m. The parametric form of the storage-flux or constitutive relationships for the proposed model is determined from numerical experiments in a simple hillslope flow geometry.

It can be said that the fundamental equation of hydrology is the water balance or conservation of fluid volume

$$\frac{dV}{dt} = I - Q \qquad (1)$$

where V represents the global fluid storage volume, I the volumetric input and Q the volumetric discharge or output. For a hydrologic system with interacting physical processes, (1) can be written in state-space form:

$$\frac{dS}{dt} = f - g \qquad (2)$$

where the state variables or storage components form a vector $S = \{S_1, S_2, \ldots S_v\}$; the vectors $f = \{f_1, f_2, \ldots f_n\}$, and $g = \{g_1, g_2, \ldots g_n\}$ represent the various input-output flux components to and from each state. Both f and g are in general, functions of the system states, S.

Although the state-space framework offers a simple representation of the system dynamics, the particular form and meaning of the inputs, outputs and states must be made explicit. The interpretation of (2) as a conservation statement for the system implies that the state variables are formed by integration over an appropriate flow volume for each state, and that the observables are defined as volume averages. Likewise, the flux quantities represent integrations of the distributed flow over the surfaces separating the states. The relationship between the surface fluxes and states represent the constitutive relations for the system. In the next section an integral-balance formulation is developed at the hillslope scale which represents the elemental spatial scale for

predicting runoff in complex terrain. Besides developing the basic model equations this section outlines the physical processes which relate storage to flux and define the constitutive relations of the model.

The integral-balance for the hillslope-stream-reach in state-space form can be written:

$$\begin{aligned}\frac{dS_1}{dt} &= f_{01} - g_{12} - f_{10} \\ \frac{dS_2}{dt} &= f_{02} - g_{21} - g_{23} - f_{20} \\ \frac{dS_3}{dt} &= q_{03} + g_{23} - q_{30}\end{aligned} \qquad (3)$$

where

S_1 = unsaturated moisture storage
S_2 = saturated moisture storage
S_3 = channel storage
f_{01} = incoming boundary flux to S_1
f_{10} = outgoing boundary flux from S_1
f_{20} = outgoing boundary flux from S_2
f_{02} = incoming boundary flux to S_2
$g_{23} = -g_{32}$ = groundwater - channel flux $S_2 \Leftrightarrow S_3$
$g_{21} = -g_{12}$ = recharge flux $S_1 \Leftrightarrow S_2$
q_{03} = upstream inflow to channel reach
q_{30} = downstream outflow from reach

The double subscripts on boundary flux quantities define the predominant sense of the flow direction as from-to (0-exteranl environment, 1-unsaturated storage, 2-saturated storage, 3-channel storage). For example the subscript 01 refers to a flow from the environment directed to state 1 (infiltration). The next section deals with the relation of state variables to flux rates for the hillslope system and the numerical experiments carried out to define each relationship.

Numerical Experiments and Development of Flux-Storage Relationships

The integration of the local equations removes the infinite dimensionality associated with continuously varying parameters and variables in space (as in the PDEs), and also provides a hydrologically useful scale for modeling - that of the hillslope. The effects of local processes and

local spatial heterogeneity on integral hillslope response must be parameterized through the integral-scale constitutive relations, that is, "effective" representations of such processes are required. The ability to simulate at spatial scales less than that of the hillslope is obviously lost; however, as a practical matter such detail is usually unnecessary in modeling fluxes relevant to water resource management.

To develop the model, one needs to determine how the integrated moisture state variables are related, i.e., the equilibria, for typical hillslope geometries. In addition, the form of the integral constitutive relations for hillslope fluxes $f(S_1,S_2)$ and $g(S_1,S_2)$ must be developed. Given such relations, the system (3) becomes a low-dimensional, physically-based model of hillslope-stream-reach hydrology.

The key to formulating a useful model from the integral-balance structure, is the determination of appropriate hillslope or catchment-scale constitutive relations. By incorporating these relations into the integral-balance, the model becomes system-specific. The approach we have taken (Lee,1993; Duffy, 1996; Brandes, 1998) is to base these relations upon steady-state numerical solutions of Richards' equation over a hillslope domain. Implicit in this approach is the assumption that the dynamics far from equilibrium are in some sense similar to those near equilibrium, and can be represented by the steady-state storage-flux relations

Approach

Richards' equation in pressure-head form (1) is solved over a two-dimensional discretized hillslope domain using the galerkin finite element code FEMWATER (Yeh, 1987). The nonlinear matrix of element equations is linearized by guessing initial values for $\{\psi\}$, and then is solved directly by Gaussian elimination. New values of $\{\psi\}$ are estimated using under-relaxation, and the procedure is repeated until convergence (ψ to within 0.0001 meter) is achieved. For approximating the time derivative, the fully implicit method was used. Further details of the numerical method are contained in Lee (1993).

The experiments involve steady-state solutions for a range of constant precipitation rates to cover the full range of hillslope saturation. Precipitation is applied uniformly to the hillslope. The numerical runs were made from an arbitrary initial condition, usually a constant pressure head throughout the domain. For each experiment, the integrated moisture state variables S_1 and S_2 are determined numerically by summing over the saturated and unsaturated hillslope volumes. The steady-state position of the water table and associated surface saturated area are also determined during the experiment. In addition, the code provides total flux rates through the various boundaries (stream, seepage, infiltration). Note that at steady-state, the subsurface flux rate will generally not equal the precipitation rate applied, due to rejection of precipitation along the saturated portion of the ground surface. This physical process, known as saturation overland flow, is an important outcome of the steady-state numerical experiments.

Hillslope geometry, boundary conditions and soil properties

The geometry used for most of our experiments is that of a convex-concave hillslope of height (H) 25 m, length (L) 100 m, and soil depth (d) of 2.5 m over an impermeable base (see Figure 1). These shape function is considered typical of hillslopes in humid-temperate regions. The surface shape function is given by (Lee, 1993):

$$h(x) = \frac{H}{e^4 - 1}\left(e^{(4 - 4x^2/L^2)} - 1\right) \qquad (4)$$

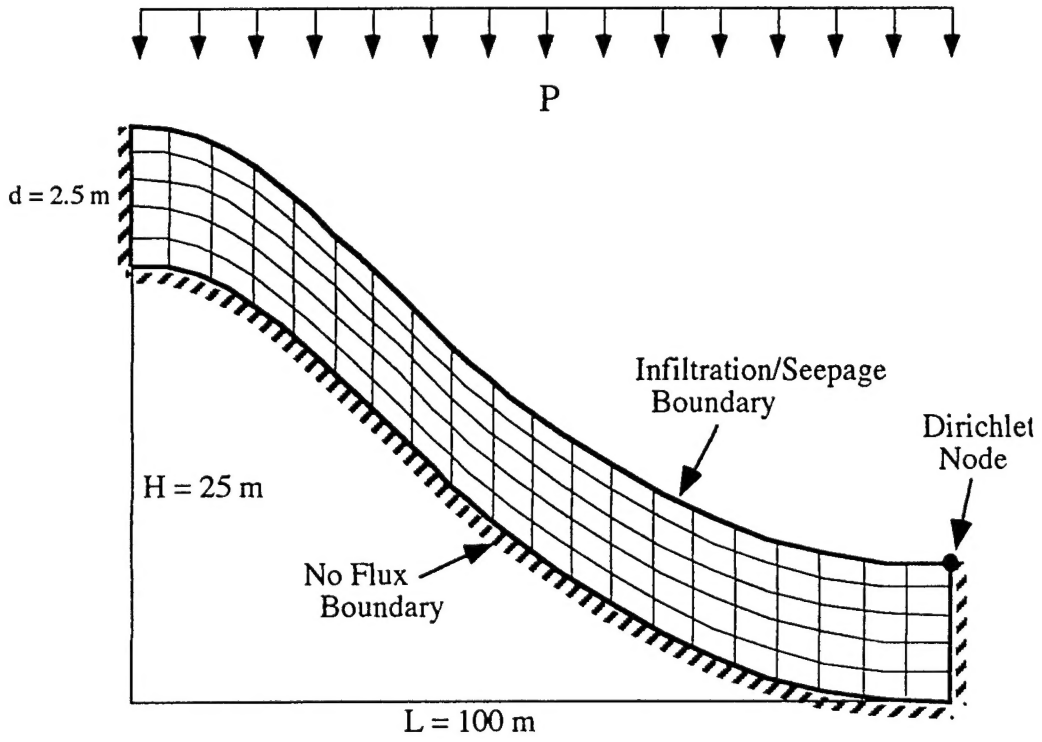

Figure 1. Schematic of the hillslope geometry and boundary conditions used in the numerical experiments (not to scale).

The domain is discretized into 4000 quadrilateral elements (4221 nodes), consisting of 200 rows by 20 columns. Thus, each element is 0.5 m long by 0.125 m high.

The boundary conditions include no-flow (Neumann) boundaries along the sides and base of the hillslope, a variable infiltration/seepage boundary along the ground surface, and a single constant head (Dirichlet) node at the foot of the slope representing a first-order stream. The no-flow boundary beneath the stream is due to converging flow from the hillslopes on opposite sides of the stream (symmetry condition), and the no-flow boundary along the base of the hillslope represents an impermeable bedrock layer.

For this report, results for three soil types are reported, a Guelph loam, a Plainfield sand, and a medium sand (Clapp and Hornberger, 1977) designated Cl&H sand. These soils represent a wide range of hydraulic characteristics. Additional soil types and hillslope geometries have been investigated by Lee (1993) and Brandes (1998), and those presented here reflect the general results. The numerical code requires input of analytical functions or tabular data describing soil moisture content, soil moisture capacity, and unsaturated hydraulic conductivity as a function of pore pressure. Analytical soil hydraulic property functions were generally used in the numerical model; however, in some cases (very low precipitation rates, highly permeable soils) tabular input was necessary for numerical convergence. For the Guelph loam and Plainfield sand, soil hydraulic properties were described by the nonhysteretic Elrick et al. (1990) parameterizations:

$$\theta(\psi) = \frac{c_1 c_2}{c_2 + |\psi|^{c_3}} + c_4 \qquad (5)$$

$$K(\psi) = K_{sat}\, e^{-k\psi} \qquad (6)$$

where θ, ψ, and K are defined as previously, K_{sat} is the saturated hydraulic conductivity, and c_i and k are fitting parameters. For consistency, the Cl&H sand property data were also fitted to these parameterizations rather than the method used by Clapp and Hornberger (1977). Table 1 summarizes the soil property parameter values used in the numerical experiments:

Soil Type	K_{sat} (cm/s)	θ_s	k (m^{-1})	c_1	c_2	c_3	c_4
Guelph loam	3.67e-04	0.523	3.36	0.243	0.421	2.0	0.28
Plainfield sand	3.44e-03	0.477	13.06	0.377	0.00154	4.0	0.1
Cl&H sand	1.76e-02	0.395	6.24	0.323	0.927	0.85	0.086

Table 1 Summary of soil property data used in the numerical experiments.

The selected soils cover a range of almost three orders of magnitude in conductivity and a wide range in porosity. The water retention and relative conductivity functions are shown in Figure 2. Note that the Guelph loam retains significantly more moisture than the sands, and thus shows a gradual decrease in conductivity with pore tension, while the Plainfield sand exhibits the characteristics of a uniformly-graded soil, with moisture content and conductivity dropping sharply over a narrow range of pore tension. The Cl&H sand hydraulic behavior is intermediate to the Guelph and Plainfield soils. Note that channel stage effects are included in these experiments and thus the emphasis is on developing relationships for the soil moisture and saturated storage.

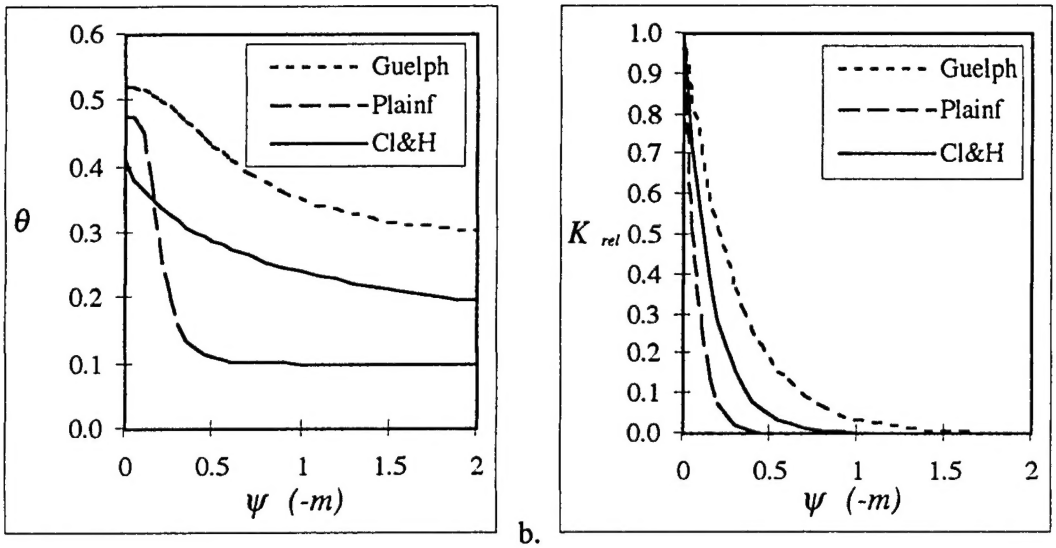

Figure 2 a) Soil moisture characteristic curves, and b) hydraulic conductivity functions for the Guelph loam, Plainfield sand, and Cl&H sand ($K_{rel} = K(\psi)/K_{sat}$).

Results

Results for the Guelph loam soil are shown in Figure 3. The first plot (a) shows the steady-state relation S_1*-S_2* , developed over a range of precipitation rates, i.e., the fixed points for different values of precipitation p. Note that the * indicates that the depth of storage is made dimensionless by the 'd' the depth of the soil. The * is dropped in later plots. The second plot (b) shows S_1 and S_2 against f_{01}, the net steady flux through the hillslope. The third plot (part c) shows fractional saturated surface area (fr_{SSA}) against S_2. Similar results were obtained for the other soil types.

A fundamental result of these numerical experiments is the competitive or inverse relationship between the moisture state variables over most of the range of soil moisture, except when the water table is at or near its lowest state (see Figure 3a). The form of this relationship can be understood in the following way: the hillslope contains a fixed volume of pore space, that must be shared by the saturated moisture (S_2), the unsaturated moisture (S_1), and the empty (air-filled) pore space. Thus, except where the empty pore volume is large, there is an inverse or competitive relationship between S_1 and S_2. This general structure is seen for a variety of soil types and hillslope configurations (Lee, 1993; Brandes, unpublished). Based on extensive numerical experiments, the flux-storage or integral constitutive relations are found to be nonlinear.

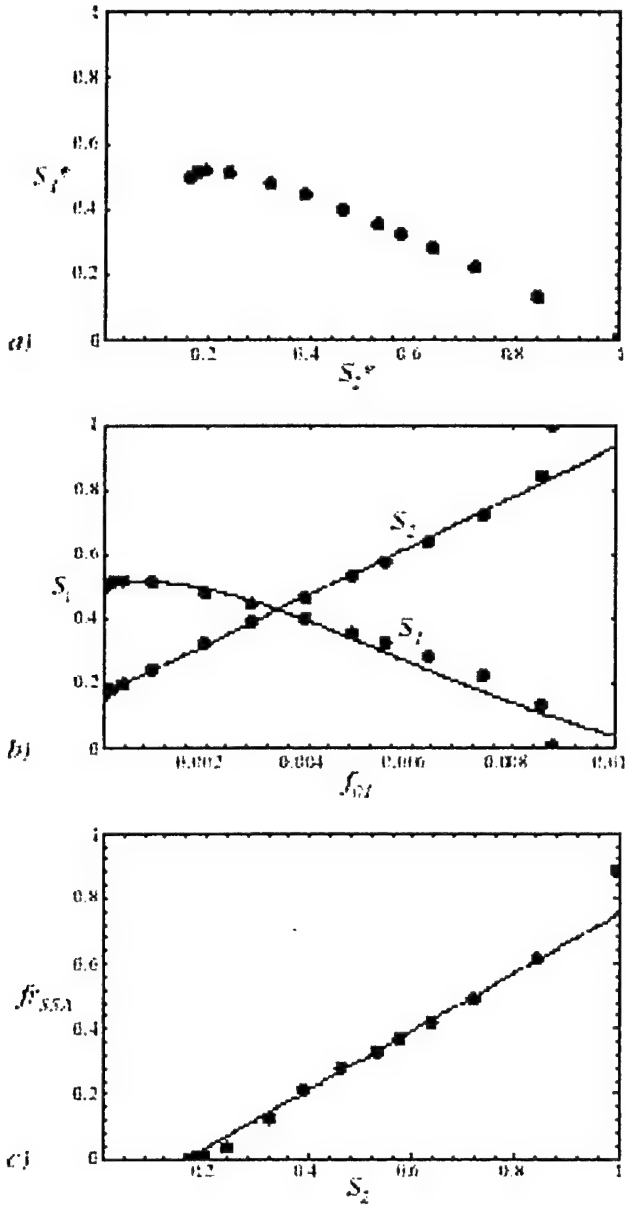

Figure 3 Numerical experiment results for the Guelph loam hillslope: a) fixed points fir , b) flux-storage relations, and c) saturated surface area-storage relation. f_{01} is the steady flux rate through the hillslope; fr_{SSA} is the fractional surface saturated area. Fits to the model are shown as solid lines.

The fitted two-state variable model

Duffy (1996) parameterized the results shown in Figure 3 above, and developed the following forms for the flux terms of for a two-state model (no channel storage):

$$f_{01} = p\left[1 - d_4(S_2 - S_2^o)\right] \quad (7)$$

$$g_{12} = d_0(S_1 - S_1^o) + d_1(S_1 + d_2)(S_2 - S_2^o)^2 \quad (8)$$

$$f_{20} = d_3(S_2 - S_2^o) \quad (9)$$

The form of the model becomes:

$$\frac{dS_1}{dt} = p\left[1 - d_4(S_2 - S_2^o)\right] - d_0(S_1 - S_1^o) - d_1(S_1 + d_2)(S_2 - S_2^o)^2 \quad (10a)$$

$$\frac{dS_2}{dt} = d_0(S_1 - S_1^o) + d_1(S_1 + d_2)(S_2 - S_2^o)^2 - d_3(S_2 - S_2^o) \quad (10b)$$

where p is the precipitation rate, S_1^o and S_2^o represent residual storage ($p = 0$), and the d_i's are fitted parameters. The term f_{01} is the net infiltration to the hillslope. This "effective precipitation" is inversely proportional to the extent of surface saturation, which is itself a linear function of saturated storage. The rejected precipitation $p_{ex}=(p - f_{01})$ becomes ssurface runoff to the channel, and thus the model represents the mechanism of saturation-excess runoff in addition to subsurface flow. Outflow from the hillslope (f_{20}) is shown to be a function of saturated storage (linear in eq.9). The steady-state rescharge rate g_{12} contains a nonlinear coupling for the two state variables. The justification for this form of the model is that it is consistent with the numerical experiment results and is of low order (Duffy, 1996); however, other forms of the model are certainly possible, for instance quadratic or cubic external flux relations. The fluxes f_{10} (evaporation) and f_{02} (leakage into the saturated zone) were not included in these numerical results and will be developed in a later section.

The physical meaning of the model parameters can be generally deduced from the flux terms (7) - (9). These parameters can be thought of as integrated versions of the parameters describing the $C(\psi)$ and $K(\psi)$ relationships of Richards' equation at the local scale. The parameters d_0, d_1, and d_2 describe the form of the moisture relation $S_1(S_2)$, which is a function of soil hydraulic properties and hillslope geometry. Parameter d_3 is a rate constant for subsurface flow, which depends on hillslope geometry and soil hydraulic conductivity. Parameter d_4 describes the relation between surface saturation and saturated storage, a function of hillslope geometry.

In terms of the saturated zone, this physically-based formulation is not unlike TOPMODEL of Beven and Kirkby (1979), which includes the processes of infiltration and saturated storage, surface runoff from saturated areas (quick flow response), and subsurface runoff (delayed response). However, in their model, infiltration simply cascades to the saturated zone when a threshold is reached. In contrast with (7) the competitive and nonlinear cross term for recharge is a critical component of the model, providing two-way coupling between the unsaturated and saturated dynamics consistent with the physics of recharge and relaxation of the water table surface (Duffy, 1996).

Macropore Flow and Hillslope Dynamics

Numerical experiments carried out by Brandes (1998) and Lee (1993) for unsaturated-saturated flow on hillslopes using classical parameterizations of matrix soil hydraulic properties, indicate excessively long response/relaxation times in comparison to similar field soils. Apparently the hydraulic properties of field soils are much smaller than the integrated effective conductivity of

the hillslope or watershed. We attribute this significant "error" to "macropore" flow in the field soils, that is, flow through interpedal cracks, root holes, or other channels of biological origin not accounted for in the soil matrix hydraulic conductivity. Further, recent data for macroporous soils suggest hydraulic conductivity functions ($K(\psi)$) often have a sharp increase in conductivity near saturation and an overall bimodal appearance of the $K(\psi)$ relationship.

A simple method is devised for estimating such hydraulic conductivity functions for macroporous soils, conceptualizing the soil as an equivalent porous medium with pore-size-weighted effective conductivity. The method requires a macropore size density function and macroporosity estimate, in addition to the matrix hydraulic conductivity function and total porosity. The resulting effective $K(\psi)$ functions are then used to numerically model variably saturated flow on a hillslope. The numerical experiments suggest that the presence of macropores: 1) increases the steady-state moisture storage in the unsaturated state; 2) increases the steady outflow rates from saturated storage in proportion to the increase in effective saturated conductivity; 3) decreases the subsurface storm response time (time to peak); and 4) significantly alters the shape of the storm hydrograph and the relative contributions of surface and subsurface flow. A brief discussion of the method and results is presented next.

"Macropore" flow through litter, structured soils or biologically-induced channels is quite common on forested slopes (Beven and Germann, 1982). Observations of rapid subsurface response at many humid forested watersheds (see for example Hursh, 1936; Hursh, 1944; Whipkey, 1965) and a semiarid hillslope site (Wilcox et al., 1997) suggest that macropore flow is an essential component of the runoff response of upland watersheds. Moreover, fitting of recession flow data from small watersheds to lumped-parameter hydraulic models (by inverse methods) has resulted in basin-scale effective saturated conductivity values approximately one to two orders of magnitude greater than indicated by available laboratory measurements (Zecharias and Brutsaert, 1988; Troch et. al., 1993).

We first develop a simple, yet physically-based parameterization of the hydraulic conductivity function for macroporous soils. The approach taken here is to modify the matrix $K(\psi)$ function to include the effect of macropore flow near saturation. Since the focus is on hillslope-scale behavior, the continuum or "equivalent porous medium" approach is used rather than treating the macropore domain explicitly (e.g., Barenblatt et al., 1960; Beven and Germann, 1981).

Next the composite or effective conductivity functions are tested using numerical experiments to assess the effect of macropore soil properties at the hillslope storage and flow. Of primary interest are the effects on moisture equilibria, outflow time scales, surface and subsurface runoff response. The numerical experiments include steady-state and dynamic conditions, a convex-concave hillslope, two distinct soil types, with two levels of macroporosity. Results are compared to those for the same soils without macropores.

The method is based on the following simplifying assumptions:

- During conditions when macropore flow is occurring (soils near saturation), the pressure in the matrix and macropores is equal. Therefore transient local conditions, such as water flowing into the macropores from the surface and then diffusing into the surrounding matrix, are not explicitly considered.
- The above assumption implies that pressure equilibration occurs rapidly as water flows within the two pore domains.
- The macropores are idealized as interconnected capillary tubes, which transmit flow only when the pore tension is less than the air entry suction value. Film flow along macropore walls and the potential effects of pore channel tortuosity are not considered here.

Under the conditions stated above, one can define an effective hydraulic conductivity (K_{eff}), which is a porosity-weighted average of the matrix conductivity and the macropore conductivity:

$$K_{eff}(\psi) = fr_{MP}\, K_{MP}(\psi) + (1 - fr_{MP})\, K_{MX}(\psi) \qquad (11)$$

where fr_{MP} is the fraction of the total porosity composed of macropores, K_{MP} is the conductivity of the macropore network, and K_{MX} is the conductivity of the soil matrix. Both K_{MP} and K_{MX} will be functions of the pore tension ψ: for the matrix through a known $K_{MX}(\psi)$ relationship (as determined in the laboratory), and for the macropores through capillarity, which will govern the pore sizes which are saturated and thus transmitting water at a given tension. Principles of hydraulics of flow in cylindrical tubes are used to calculate hydraulic conductivity of the macropores (similar to the approach used by Chen and Wagenet, 1992).

To apply these equations, two additional pieces of data are required: the macroporosity fraction fr_{MP} and a macropore pore size distribution or density function $f(r)$. Values of 0, 0.001, and 0.01 were used for fr_{MP} to represent a full range of reasonable values. Various studies have found that numbers of soil pores of a given size class are inversely proportional to pore size (e.g., Wilson and Luxmoore (1988) infiltrometer data). Therefore, an exponential probability density function was used:

$$f(r) = k_1 \exp(-k_2 r) \qquad (12)$$

where r is the pore radius, and k_1 and k_2 are fitting parameters. Since the area under the density function $f(r)$ must integrate to unity, the parameters k_1 and k_2 are interdependent (furthermore, approximately equal for k_1 and $k_2 > 1$). The sensitivity of K_{eff} to these parameters was assessed, and it was determined that the effect was small in comparison to the value used for fr_{MP}. For the results shown here, the values $k_1 = 0.63$ and $k_2 = 0.6$ were used with a macropore radius range of 0.01 to 2.5

mm. The 0.01 mm radius corresponds to a ψ_{ae} value of -1.5 m; below this value, flow is assumed to occur only in the matrix domain.

Given the function $f(r)$, the weighted macropore conductivity is calculated using the following equation:

$$K_{MP}(\psi) = \frac{\int_0^{r^*} K_{MP}(r) f(r) dr}{\int_0^{r^*} f(r) dr} \qquad (13)$$

with r^* chosen such that $\psi_{ae}(r^*)=\psi$, that is, the weighted sum includes only those pores (with $r < r^*$) which are contributing to flow at a given value of ψ. This integral is evaluated discretely for increasing pore tensions (decreasing values of r^*), starting from saturated conditions where all pores are contributing flow.

Matrix soil properties

Two soil types were used in the K_{eff} calculations and simulations, a Guelph loam and a Plainfield sand. The Guelph loam has finer-grain size, and retains significantly more moisture than the sand, and thus shows a gradual decrease in conductivity with pore tension. The Plainfield sand exhibits the characteristics of a uniformly-graded soil, with moisture content and conductivity dropping sharply over a narrow range of pore tension between –0.1 m and –0.5 m. The $K_{MX}(\psi)$ functions for the unsaturated soils is represented by the exponential Gardner relation:

$$K_{MX}(\psi) = K_{sat}\, exp(-\alpha \psi) \qquad (14)$$

where $K_{sat} = 3.67\text{x}10^{-4}$ cm/sec and $\alpha = 3.36$ m^{-1} for the Guelph loam, and $K_{sat} = 3.44\text{x}10^{-3}$ cm/sec and $\alpha = 13.06$ m^{-1} for the Plainfield sand (Elrick, 1990). These two soils bracket the threshold saturated conductivity value of 10^{-3} cm/sec for subsurface storm flow, suggested by Freeze (1972).
Once the composite conductivity functions were developed, the galerkin finite element code FEMWATER [*Yeh*, 1987] was again used to solve Richard's equation over a two-dimensional hillslope domain as described earlier.

Steady-state results for the two soil types and three values of macropore fractions (f_{mp}=0.0, 0.01 and 0.001) are shown in Figures 4 through 7. Figures 4 and 5 show the steady-state integrated moisture (S_2*, S_1*) and storage-flux ($q(S_2)$) for a range of constant precipitation rates, and shows the expected inverse relationship between saturated and unsaturated moisture, except under dry conditions, as discussed previously by Duffy (1996) and Brandes et al. (1998). We note that although the soil moisture retention curve $\theta(\psi)$ is unchanged by the macropore parameterization, there is a significant effect on the unsaturated-saturated storage, since this depends on the overall

rate of flux through the hillslope. In particular, for macropore flow, higher flux rates and a lower water table are observed within the saturated zone to balance the increased steady flux rate through the hillslope . The lower water table leads to an overall higher moisture storage in the unsaturated zone.

The effect of macropore flow is most pronounced for the Plainfield sand (Figure 5). For fr_{MP}=0.01, the relation attains a maximum with relatively flat slope over intermediate values of S_2. In this case, the macropore conductivity increases over the same range of pore pressure where moisture content changes rapidly in the soil moisture characteristic $\theta(\psi)$. Therefore, relatively large increases in S_1 are required to increase the unsaturated hydraulic conductivity necessary to transmit the macropore-enhanced fluxes.

Under very dry conditions and with macropore flow, the numerical solutions for both soils did not converge near the peak of the soil moisture storage . This is due to the highly nonlinear effective conductivity relations, and to the presence of weakly damped equilibria (see discussion in Brandes et al., 1998).

The steady flux data are shown in the lower portion of Figures 4 and 5, give the subsurface flux rate as a function of the saturated storage S_2. The steady flux rates for the Guelph loam hillslope increase by about an order of magnitude for fr_{MP}=0.001, and by two orders of magnitude for fr_{MP}=0.01. The effect is less pronounced for the Plainfield sand. Note that the steady-state fluxes are not equal to the applied precipitation rate, due to rejection of infiltration along the saturated surface near the stream. This relationship between the extent of surface saturation and saturated storage is determined by hillslope geometry and boundary conditions, and is not effected by macropores.

It is clear that the subsurface flux rates are greatly enhanced by macropore flow as parameterized here. Interestingly, this effect is apparently proportional to the effective saturated conductivity of the hillslope. Figure 6 shows the combined data from Figures 6 and 7, with each curve scaled by the associated $K_{eff\text{-}sat}$ value. Note that the data fall very close to a single curve, except at very high levels of saturated storage (S_2>0.8). Note that the flux -storage relation now requires a nonlinear function and we adopt the form:

$$q / K_{sat} = \left[c_1 (S_2 - S_2^0) + c_2 (S_2 - S_2^0)^2\right] \qquad (15)$$

where c_1 = 0.0105, c_2 = 0.0032 , and S_2^0 = 0.166 for these data. The c_i can be thought of as rate constants, and the parameter S_2^0 describes the residual moisture storage (corresponding to p=0).

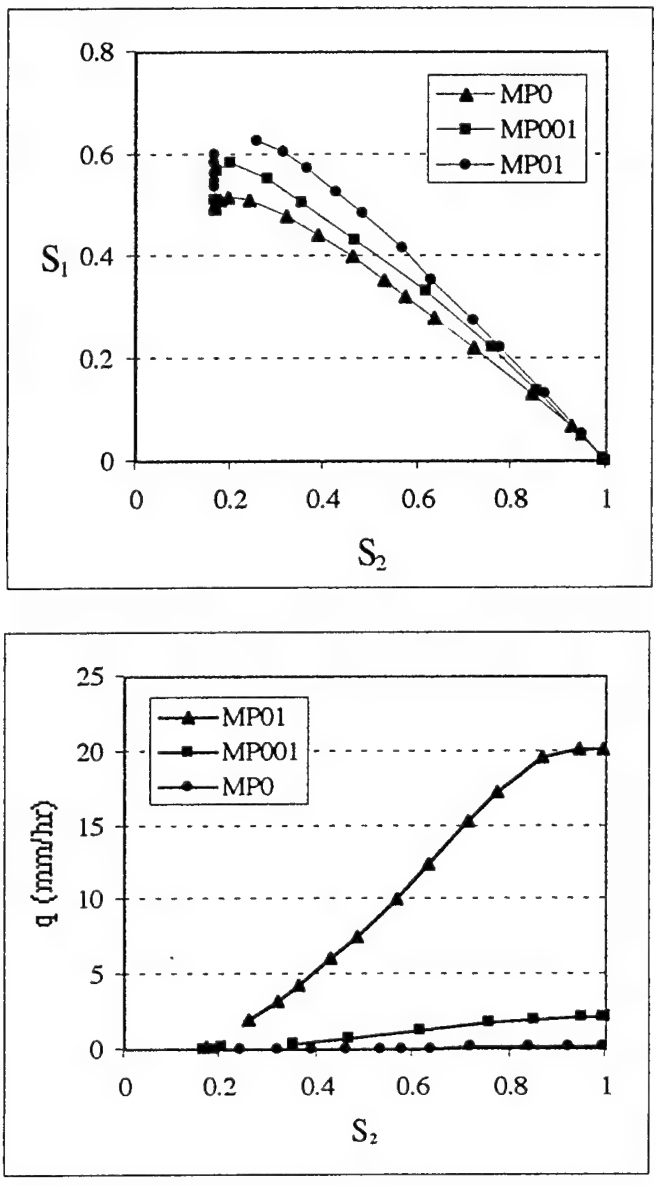

Figure 4. . Saturated-unsaturated storage (upper plot) and the subsurface for the Plainfield sand for 3 values of macropore flow fr_{MP}=0.0, fr_{MP}=0.01 and fr_{MP}=0.001, (after Brandes and Duffy, 2000).

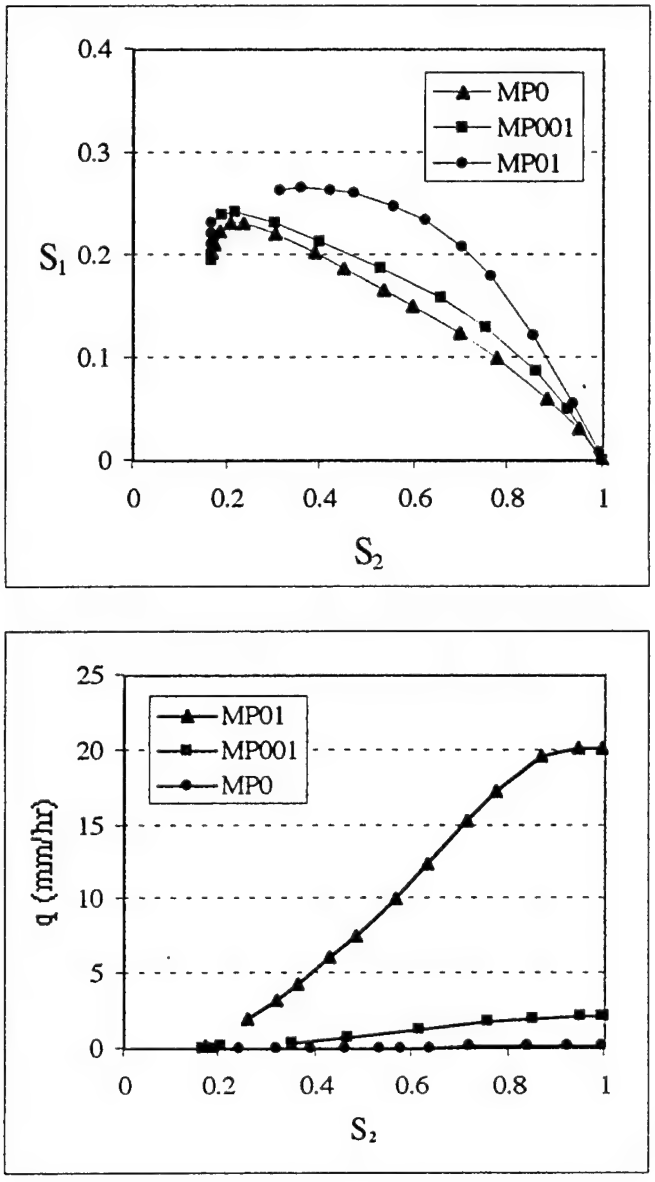

Figure 5. Saturated-unsaturated storage for the Guelph loam for 3 values of macropore flow fr_{MP}=0.0, fr_{MP}=0.01 and fr_{MP}=0.001, (after Brandes and Duffy, 2000).

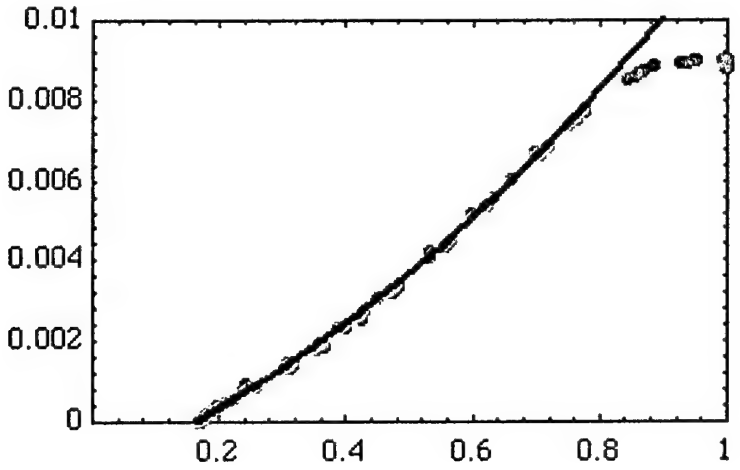

Figure 6. Scaled data for both soils based on equa. (14) $q / K_{sat} = f(S_2)$ (after Brandes and Duffy, 2000).

Evaporation and Transpiration

The two-state integral-balance model for unsaturated-saturated flow (Duffy,1996) is extended to study the timing of atmosphere-controlled and soil-moisture controlled evaporation for sloping topography. The modeling strategy is to construct the state-space for unsaturated-saturated storage by direct integration of the unsaturated-saturated flow equations (Richards' equation) and to devise a parametric model for evaporation. An empirical evaporation equation is proposed, which is a function of both the unsaturated and saturated state variables. The dynamical system now takes the form

$$\frac{dS_1}{dt} = f_{01} - g_{12} - e_{10}$$
$$\frac{dS_2}{dt} = f_{02} - g_{21} - e_{20} - f_{20} \qquad (16)$$

For the saturated surface ($\beta(S_2)$) evapotranspiration flux is subject to "atmospheric" control and e_{20} is simply defined as the product of the potential evaporation p_e and ($\beta(S_2)$):

$$e_{20} = p_e \beta(S_2) \qquad (17)$$

Evapotranspiration flux over the unsaturated surface of the hillslope is assumed to be controlled by the soil moisture and is defined as product of p_e, the fraction of the hillslope that is unsaturated and the soil evapotranspiration function $w(\chi)$:

$$e_{10} = p_e(1-\beta(S_2))\cdot w(\chi) \qquad (18)$$

The soil moisture evapotranspiration function $w(\chi)$ is a weighting function (0,1) defined as:

$$w(\chi) = \frac{(1+a\,\chi)\chi^m}{a+x^m}; \quad \chi = \frac{S_1}{d\cdot n - S_2} \qquad (19)$$

The function $\chi(S_1,S_2)$ represents the degree of saturation of the unsaturated volume, d the average depth of the soil and m determines the shape of $w(\chi)$. The formula of Thornthwaite [1948] relates potential evapotranspiration to temperature ($ET_p \propto T^{\alpha}$) where T is the mean daily air temperature For simplicity, the potential ET is expressed as the power function of the daily maximum temperature,

$$ET_p = b_1\left(\frac{T}{T_{\max}}\right)^{b_2} - b_3 \qquad (20)$$

The ET model results suggest that the extent and timing of surface-saturation during cycles of wetting and drying is dependent on the saturated (storage) of the watershed, which in turn is closely tied to the soil moisture storage and the magnitude of surface and subsurface runoff components. The transition from atmosphere-controlled evaporation to soil-controlled evaporation following precipitation is examined for a range of soil types and hillslope geometries. This transition may be abrupt or smooth depending on the parametric form of the evaporation term and the overall storage characteristics of the terrain.

Snow Accumulation and Melt

A simple model for daily potential snowmelt model was developed by the U.S. Army Corps of Engineers and described by Singh, [1992] and have adapted the model here. The basic idea is that the potential flux due to snow melting is a simple function of air temperature

$$M = 0.4(T - T_{melt}) \qquad (21)$$

where T is the daily maximum air temperature, M [mm/day] is the potential snowmelt at T [°F]and T_{melt} is the local melt temperature. The range of T_{melt} is from 27 to 42 [°F] which corresponds to open and forested sites.

Based on the potential snowmelt relation (21), the accumulation and melt of snow and the relation to infiltration is formed by the following conditional statements:

$$P_m(t) = f(P_s,t), \text{ if } T \geq T_{melt} \quad (23)$$

$$P_m(t) = 0, \text{ and } P_s(t) = P_s(t-1) + P(t), \text{ if } T \leq T_{melt} \quad (24)$$

$$f(P_s,t) = M \text{ and } P_s(t+1) = P_s(t) - M, \text{ if } M \leq P_s(t) \quad (25)$$

$$f(P_s,T) = P_s(t) \text{ if } M \succ P_s(t) \quad (26)$$

where P_m(t) is the snowmelt at time t, P(t) is the precipitation at time t and P_s(t) is the amount of the accumulated snow-pack at time t. At any time, precipitation is the sum of rainfall and snowmelt.

Space-Time Decomposition and Dimension Estimation

Multichannel SSA is a space-time version of the Karhunen-Loève theorem and a general discussion of the method is provided by Plaut et al. (1994). The method is widely used to identify coherent space-time patterns from historical observations at regular and irregular locations. Unlike traditional spectrum analysis, where the basis functions are sine and cosines, SSA is determined from estimates of the lagged cross-covariance (space and/or time) where basis functions are data-adaptive, empirical and orthogonal. The method can be shown to be optimal in the sense of capturing the maximum variance with the fewest independent components. The goal here is to estimate periodic or nearly periodic variance components in P-T-R and relate these to hydrologic conditions across the Wasatch Front. A brief description of the method follows.

Theory

We first define an L-dimensional data vector X_{li}, $1 \leq l \leq L$, $1 \leq i \leq N$, where l is channel number representing spatial variables, i represents the time index, N is record length and the mean of each time series has been removed. The expansion of $X_{l,i}$ is given by:

$$X_{l,i+j} = \sum_{k=1}^{L \times M} A_i^k E_{l,j}^k, \quad 1 \leq l \leq L, \; 1 \leq j \leq M, \quad (27)$$

where M is the window length or embedding dimension. Thus, $X_{l,i+1}$, $X_{l,i+2}$, ..., $X_{l,i+M}$ represent shifted time series at channel l from the multichannel record $X_{l,i}$. The coefficient A_i^k is called the space-time principal component (ST-PC). The vector E^k, is defined as a space-time empirical orthogonal function (ST-EOF), and is the kth eigenvector of the block-Toeplitz matrix T_x:

$$T_x = \begin{bmatrix} T_{1,1} & T_{1,2} & \cdot & \cdot & \cdot & T_{1,L} \\ T_{2,1} & T_{2,2} & \cdot & & & \cdot \\ \cdot & \cdot & \cdot & \cdot & & \cdot \\ \cdot & \cdot & \cdot & \cdot & T_{l,l'} & \cdot \\ \cdot & & & \cdot & \cdot & T_{L-1,L} \\ T_{L,1} & \cdot & \cdot & \cdot & T_{L,L-1} & T_{L,L} \end{bmatrix} = E^T \Lambda E \qquad (28)$$

$T_{ll'}$ is the $M \times M$ lag covariance matrix between channel l and channel l' with the element $(T_{l,l'})_{jj'}$. The least-biased estimate of the element $(T_{l,l'})_{jj'}$ in row j and column j' is [Vautard et al.,1992]:

$$\left(T_{l,l'}\right)_{jj'} = \frac{1}{N-|j-j'|} \sum_{i=1}^{N-|j-j'|} X_{l,i} X_{l',i+j-j'} \qquad 1 \le j \le M,\ 1 \le j' \le M \qquad (29)$$

The ST-PCs of T_x are defined as the orthogonal projections of the original series on the ST-EOFs:

$$A = XE. \qquad (30)$$

The dimension of A is $(N\text{-}M+1)\times(L+M)$. The ST-PCs can be thought of as weighted moving averages of the original time series X.

We are mainly interested in the ST-PC's which contribute a large fraction of the variance and those which represent oscillatory components of the signal and can in some way be distinguished from the underlying noise in the record. We will revisit the question of resolving significant periodic or almost periodic components and noise later. The standard approach is to sort the eigenvalues λ_k in descending order. The plot of eigenvalue λ_k versus k represents a ranking of the relative variance contribution for each ST-PC. If adjacent eigenvalues are nearly equal and their respective eigenvectors are in quadrature, then they are assumed to be an oscillatory pair and the ST-EOF pairs are either periodic or almost periodic. The oscillatory pair would represent a sine and cosine-pair with a phase shift. We apply this approach here, inspecting the E^k's of the largest eigenvalues λ_k from which the period (frequency) is estimated for a particular channel or altitude.

The cutoff for "significant" components is arbitrarily determined to be the value of k where a flattening or change in slope of the ranked eigenvalues is observed

and the variance contribution is small. This break in slope is sometimes referred to as the "noise floor". Of course this definition is problematic since ranking of eigenvalues by size has no ordering with respect to the period or frequency content of the data, as would be the case for Fourier spectral estimates. It is possible that significant oscillatory pairs may not be detected, especially in cases where the underlying noise spectrum is from a correlated stochastic process, which is often the case in hydrologic data. Next we examine the space-time characteristics of precipitation -temperature and runoff (P-T-R) for the Wasatch Front, northern Utah, using multi-channel SSA and the qualitative approach to detecting oscillations described above.

State-Space Dimension

Multichannel SSA was applied separately to the precipitation, temperature and runoff (P-T-R) data sets. The concurrent record was from January 1948 to December 1990, representing 43 years of data. As in Fourier spectrum and covariance analysis, it is necessary to test the effect of the time embedding (M) or lag on SSA estimates. The range $140 \leq M \leq 172$ was examined and $M=160$ seemed to provide the best resolution across the range of oscillations of interest (annual to decadal). The ranked eigenvalues for each variable is shown in Figure 7. From the graph, the near equality of some pairs of leading eigenvalues is noted. These pairs often (but not always) correspond to eigenvectors that are periodic or nearly periodic and in quadrature. The analysis focuses on the first 8-10 components, up to the point where the slope of λ_k versus k flattens and the variance contribution is small. A summary of oscillatory pairs and the estimated period for precipitation, temperature and runoff is given in Table 2.

The annual oscillation represents the leading pair of eigenvalues for P-T-R as shown in Table 2. For precipitation the annual oscillation represents 31% of the total space-time variance. Annual harmonics at periods 0.5, 0.33 and 0.25 years individually contribute from 1.5-1.9% of the total variance for P. The period of 11 years accounts for 1.7% of the variance, while the interannual time scale, period 3 contributes 1.1%. In the case of temperature, the annual oscillatory pair represents 93% of the total variance and the semi-annual pair contributes an additional 1%. Interannual and decadal oscillations are all quite small, with the interannual component contributing ~0.1%.

For runoff the annual oscillation contributes 27% of the total variance of the 9 stations, while the second largest oscillatory pair is at the 11-year period with 10.5%. The seasonal harmonics contribute another 12%, while the interannual components

represent 2.6% of the total variance. Overall, we can say that the variance contribution for P-T-R at all altitudes is dominated by the annual oscillation and harmonics, precipitation shows significant but weak interannual and decadal oscillations, while runoff exhibits strong interannual and decadal oscillations.

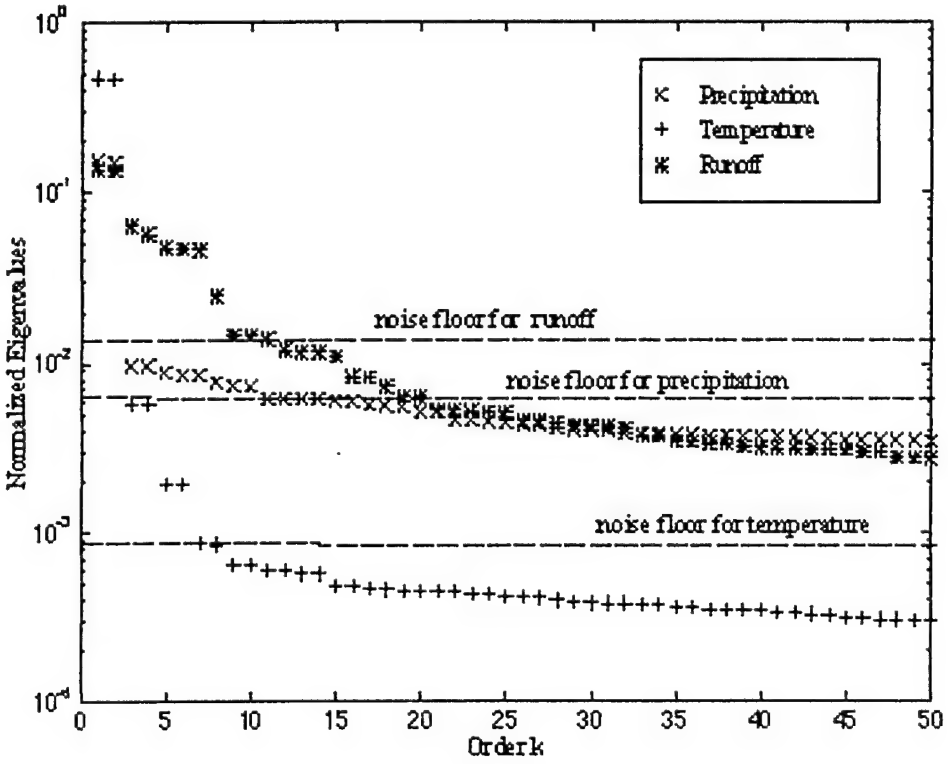

Figure 7. The eigenvalue spectrum for precipitation, temperature and runoff across the Wasatch Front, northern Utah. The "noise floor" gives a measure of the statistical dimension of the hydrologic system.

Reconstruction of the space-time structure of P-T-R

In order to get a better sense of how well the first few eigenmodes describe the P-T-R signal above the noise floor, we reconstruct the P-T-R with the first eight eigenvectors and examine the noise-free response. The reconstructed component R associated with the k_{th} ST-EOF at time i, and for channel l is given by [Plaut et al.,1994]:

$$R_{l,i}^{k} = \frac{1}{M}\sum_{j=1}^{M} A_{i-j}^{k} E_{l,j}^{k} \qquad \text{when } M \le i \le N\text{-}M\text{+}1,$$

$$R_{l,i}^{k} = \frac{1}{i}\sum_{j=1}^{M} A_{i-j}^{k} E_{l,j}^{k} \qquad \text{when } 1 \le i \le M\text{-}1,$$

$$R_{l,i}^{k} = \frac{1}{N-i+1}\sum_{j=i-N+M}^{M} A_{i-j}^{k} E_{l,j}^{k} \qquad \text{when } N\text{-}M \le i \le N \qquad (31)$$

where the range of k is from 1 to $L \times M$. A time series for any channel can be reconstructed by summing over the dominant components. Figure 8 shows the reconstructed time series of P-T-R for two channels, one at high elevation and another at a low elevation. The reconstructed temperature time series represents 95% of the total variance (4 ST-PC's) in the original data. For precipitation, seasonal harmonics and low-frequency components (10 ST-PC's) explain 37% of the total variance, while 59% of the total variance is explained for the runoff data (10 ST-PC's).

Precipitation:

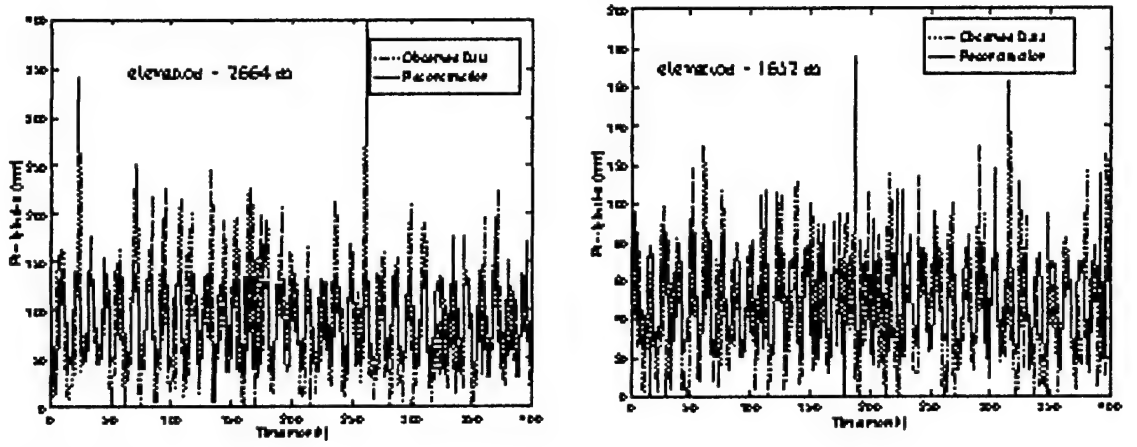

Temperature:

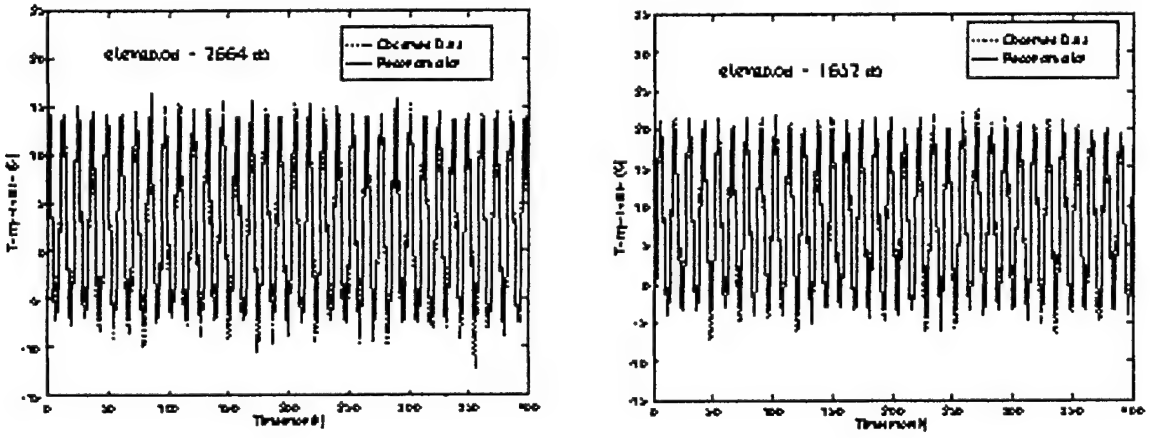

Runoff:

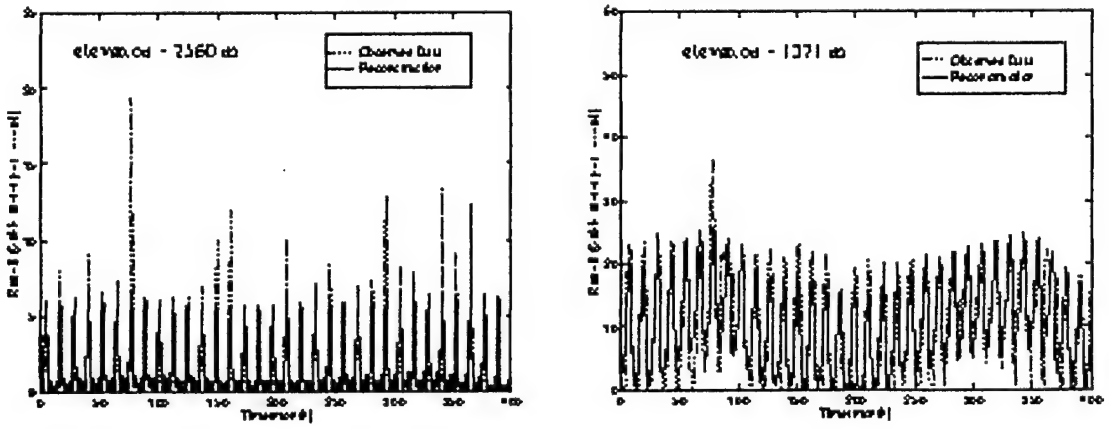

Figure 8. The reconstructed noise-free precipitation-temperature-runoff records for the Wasatch Front. The reconstructions are based on the first 8 eigenmodes of the for variable. The left-most plot is at hight elevation and the right-most plot is at low elevation.

Phase-Plane Trajectory of the Reconstructed P-T-R

The dynamic behavior of the hydrologic system can be examined by constructing the time- trajectory or parametric curve formed by using the reconstructed state variables as coordinates. Figure 9 illustrates the P-T-R trajectory at three elevations of Wasatch Range for the reconstructed time series. The variance components were the same as in Figure 8 and the period of reconstruction is 43 years. At the highest altitude the three dimensional trajectory exhibits tightly spaced loops, where each loop represents the annual oscillation. By comparison, at low elevation the phase plane is smeared out reflecting the introduction of the low-frequency components and deeper groundwater discharge. The higher elevations are clearly dominated by seasonal fluctuations while the low elevations contribute the longer time scales imparted by the characteristic hydrogeologic conditions controlling runoff.

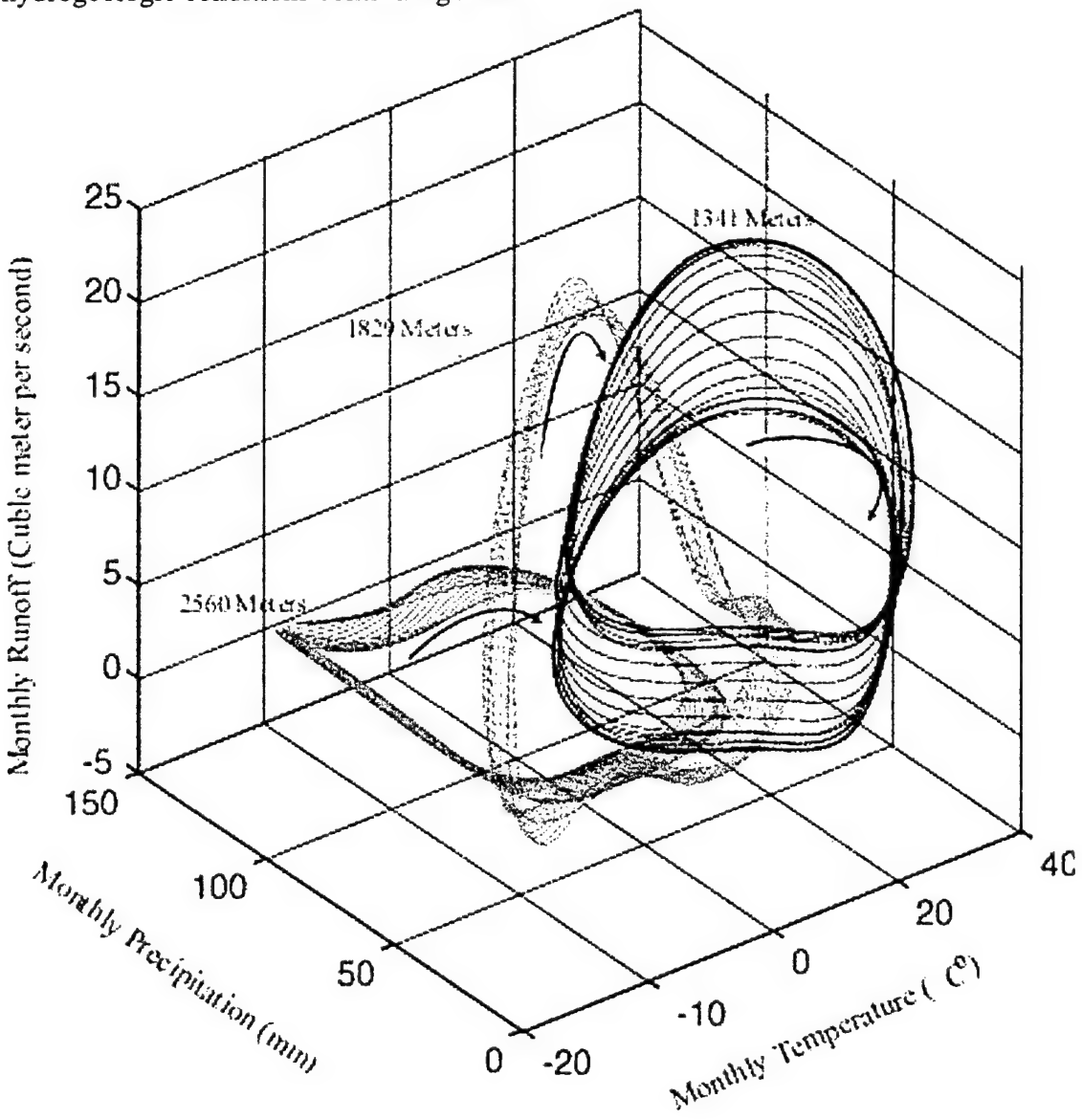

Figure 9. A phase-plane plot of reconstructed precipitation-temperature -runoff for 3 elvations. Note the low-frequency, quasi-periodic character of the lowest elevation where the long time scales of deep groundwater baseflow to streams affects the runoff.

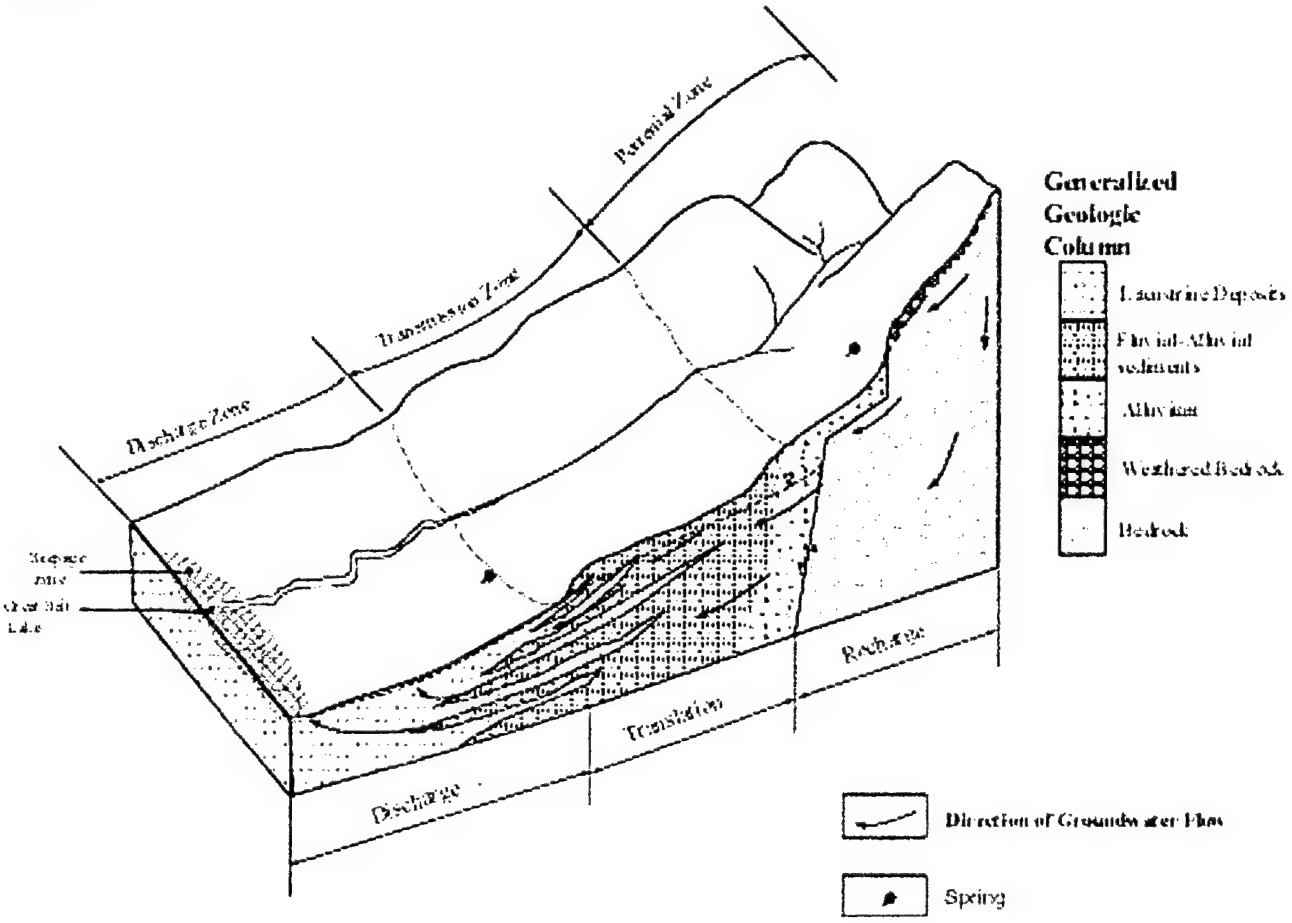

Figure 10. The hydrogeologic conceptual model for the Wasatch Front showing the relation between surface and subsurface hydrology and demonstrating the importance of the alluvial fans to supporting low-frequency contribution to streamflow at the lowest elevation..

Model and Parameter Identification

LDMS applies the Genetic Algorithm (Holland,) to the problem of model and parameter identification. There are many system identification techniques that have been used to build accurate mathematical models of dynamic systems. These are generally based least mean squares or maximum likelihood fitting of model to data, and most are some sort of gradient-guided local search techniques [Tan, et al., 1995]. These conventional techniques require a smooth search space and easily fail in obtaining the global optimum when the search space is not differentiable. Furthermore, they are not easily be applied to nonlinear systems and are not valid if the nonlinearities of the

system are not differentiable such as with threshold nonlinearities. Genetic Algorithms (GAs) are based on the metaphor of natural selection and Darwinian evolution. Genetic Algorithms simultaneously search the solutions through multiple points in the solution space and often are found to be the most effective method of finding the global optimum.

The optimum parameters are determined in such a way that the sum of squares of the difference between the actually observed and the modeled values, multiplied by a number that measures the degree of precision, is a minimum. This function is called the fitness function is given by:

$$f = \exp\left\{-a\sqrt{\frac{\sum_{i=1}^{N}\left[q_o(i)-q_m(i)\right]^2}{N}}\right\}. \qquad (32)$$

In our case q_o is observed runoff, q_m is modeled runoff, N is the total time steps of the simulation, i is the time index and a is a positive scaling factor. By including the exponential function, the minimization problem changed to maximum and the fitness value can be constrained to the range of (0,1].

In order to examine the accuracy of each models, we apply several forecast accuracy measures [Maidment,1993] for estimating the forecast error. The measures include (1) mean absolute error (MAE), (2) Relative mean absolute error (RMAE), and (3) mean square error (MSE) [Baidment,1993], which are defined by

$$MAE = \frac{1}{N}\sum_{i=1}^{N}\left|q_m(i)-q_o(i)\right|$$

$$RMAE = \frac{N}{\sum_{i=1}^{N} q_o(i)}\,MAE \qquad (33)$$

$$MSE = \frac{1}{N}\sum_{i=1}^{N}\left[q_m(i)-q_o(i)\right]^2$$

Field Application: West Branch, Susquehanna River Basin

Modeling the rainfall-runoff process for a hydrologic system (river basin, drainage basin, catchment or watershed) has been a central problem for contemporary hydrology research. The problem is made difficult because of the heterogeneous space-time nature of hydrologic systems. Increasingly, complex models for lareg-scale hydrological response have been developed using tools of high performance computation. However, as has been pointed out by Jakeman and Hornberger [1993], it is not necessarily true that spatially detailed complex models improve the model results and in fact

may lead to over-parameterization. That is, parameters themselves introduce noise or model errors and limit the predictability of the phenomenon.

Geohydrologic Framework

The selected research site is the Upper West Branch, which is a sub-basin of the Susquehanna River Basin. Figure 2 describes its location. This river basin is located in north central Pennsylvania and has an area of 14,710 km^2. Most of the Upper West Branch is within the Appalachian Plateau physiographic province. Only a very small portion of the south part belongs to the Appalachian Mountain section of the Valley and Ridge physiographic province. The regional dip of the bedrock rarely exceeds 25 feet per mile. Elongate, gentle folds form alternating anticlines and synclines. These gentle warps are surface expressions of small displacements along deep-seated faults. Deformation of strata in the Appalachian Plateaus is extremely subtle. Glacial erosion and deposition left a nearly continuous layer of till over upland bedrock. Colluvium and alluvial deposits mostly distribute in main valleys. In this region, unconsolidated glacial, outwash, colluvium and alluvial deposits form the upper-layer aquifer. With the enough thickness, this aquifer is mainly productive. The consolidated sedimentary rocks mainly are shales, sandstones, siltstones and coal seams, which are almost flat-lying to gently folded. The main water-yielding rocks are sandstones. The fractures, joints and pores in these consolidated rocks form the bedrock aquifers. This aquifer is constructed the lower-layer aquifer in the Upper West Branch, which is mostly overlain by the upper unconsolidated aquifer.

Figure 11. depicts the hydrogeologic conceptual model of the Upper West Branch. The water is occurring in the unconsolidated aquifers and bedrock aquifers. Most of the precipitation directly recharges into the upper unconsolidated layer. In the upper land, since the till is thin and very permeable, water in till rapidly discharges to colluvium or alluvial aquifers. In lower lands, the precipitation mainly infiltrates into colluvium and alluvial aquifers. Then groundwater in this layer may runoff to the local tributaries or streams. This forms the local flow system. However, a small part of water in unconsolidated aquifers may infiltrate down to the fractures in lower bedrock aquifers. Bedrock aquifers in the unglaciated part of the Upper West Branch accept less direct recharge from the precipitation because this part is highly dissected and much of the area is near highly sloping. The circulation of water in bedrock aquifers does not extends no more than a few hundred feet below the land surface [Harlow et al, 1993] while the permeability of bedrock aquifers decreases with depth. The small portion of the water in unconsolidated aquifer may moves vertically downward through fractures, then horizontally flows through the consolidated aquifers and finally discharges to the streams. Because of the limited flow depth, the water flow paths are typically not too long, commonly extending no more than several kilometers in their longest dimension [Seaber, et al., 1988]. The water circulation in bedrock aquifers forms the intermediate flow system. No

regional flow occurs in this basin because the thickness of the regional permeable bedrock aquifers is less than several hundred feet.

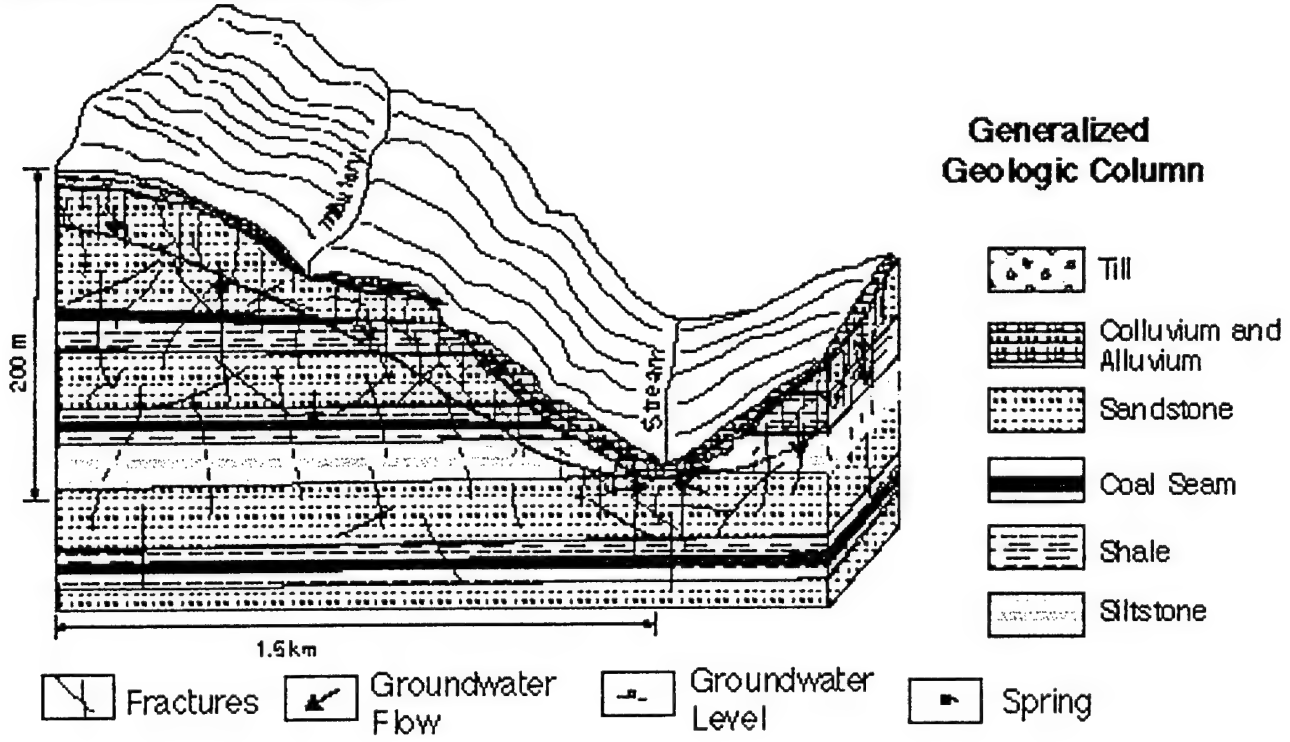

Figure 11. The hydrogeologic conceptual model for a typical stream-reach within the Upper West Branch of the Susquehanna River. Shallow till, colluvium and alluvium form the near-surface groundwater reservoir while the deeper subsurface reservoir is dominanted by fracturing in various sedimentary units.

The Model

For the hydrogeologic characteristics of the Upper West Branch, a series of coupled nonlinear integral-balance model equations were proposed (Table 1). This serves to constrain the model to up to two state variables and a minimal number of parameters. The six models of the Upper West Branch were tested and parameters estimated with the Genetic Algorithm method for observed daily precipitation, temperature and streamflow over the period July 1985 to June 1987. The modeled and observed data are depicted in Figure 12. Comparison of the results of the linear and nonlinear models, we see that the nonlinear models improve the peakflow better than the linear models. It was also determined that the two-state coupled nonlinear model best matches the observed runoff. The developed models also were verified by applying the calibrated parameters to predict the runoff in the period of July 1989 to June 1991 with the given precipitation and temperature. The predicted

results are shown in Figure 13. As for the calibration period, the model results for the two-state nonlinear integral-balance model matches the observed values best.

Model Type	Linear	Nonlinear
One-state	$s\frac{dy}{dt} = R - \alpha y;$ (16) $q_g = \alpha y;$	$s\frac{dy}{dt} = R - (\alpha y + \beta y^2);$ (17) $q_g = (\alpha y + \beta y^2);$
Two-state, uncoupled	$s_1\frac{dy_1}{dt} = \lambda R - \alpha_1 y_1;$ $s_2\frac{dy_2}{dt} = (1-\lambda)R - \alpha_2 y_2;$ $q_g = \alpha_1 y_1 + \alpha_2 y_2;$ (18)	$s_1\frac{dy_1}{dt} = \lambda R - (\alpha_1 y_1 + \beta_1 y_1^2);$ $s_2\frac{dy_2}{dt} = (1-\lambda)R - (\alpha_2 y_2 + \beta_2 y_2^2);$ $q_g = (\alpha_1 y_1 + \beta_1 y_1^2) + (\alpha_2 y_2 + \beta_2 y_2^2);$ (19)
Two-state, coupled	$s_1\frac{dy_1}{dt} = R - \alpha_1 y_1 - \gamma(y_1 - y_0);$ $s_2\frac{dy_2}{dt} = \gamma(y_1 - y_0) - \alpha_2 y_2;$ $q_g = \alpha_1 y_1 + \alpha_2 y_2;$ (20)	$s_1\frac{dy_1}{dt} = R - (\alpha_1 y_1 + \beta_1 y_1^2) - \gamma(y_1 - y_0);$ $s_2\frac{dy_2}{dt} = \gamma(y_1 - y_0) - (\alpha_2 y_2 + \beta_2 y_2^2);$ $q_g = (\alpha_1 y_1 + \beta_1 y_1^2) + (\alpha_2 y_2 + \beta_2 y_2^2);$ (21)

Table 2. List of the integral-balance models for the different conceptualized models and constitutive relationships between state variables and output flux components.

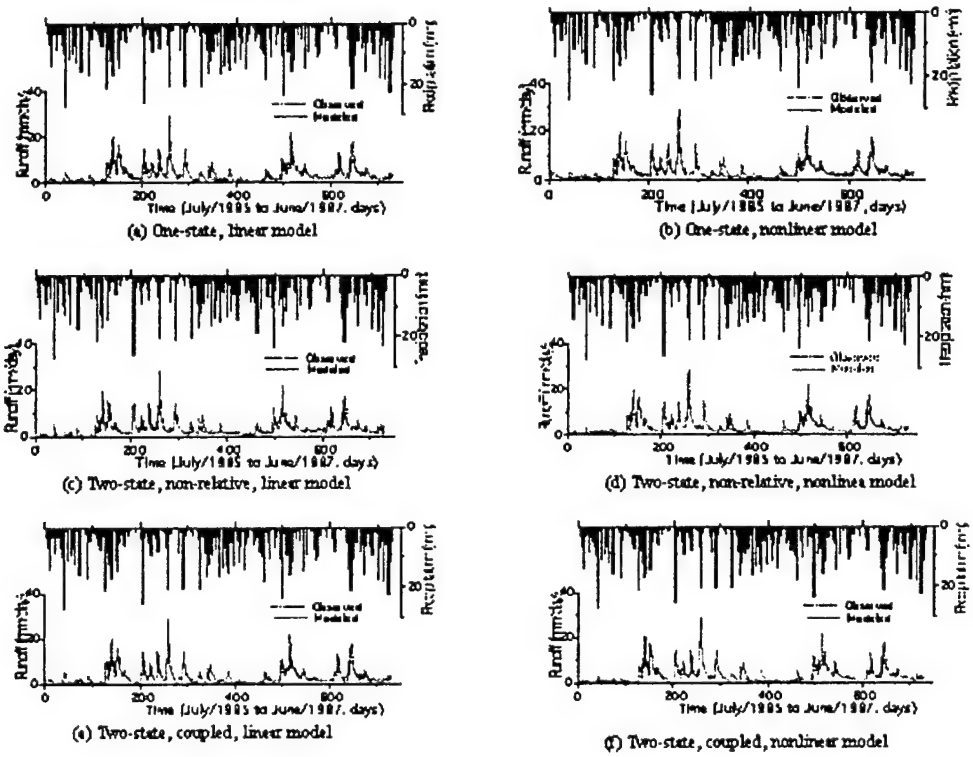

Figure 12. The modeled and observed runoff for the Upper West Branch for each of the 6 models proposed in Table ?.

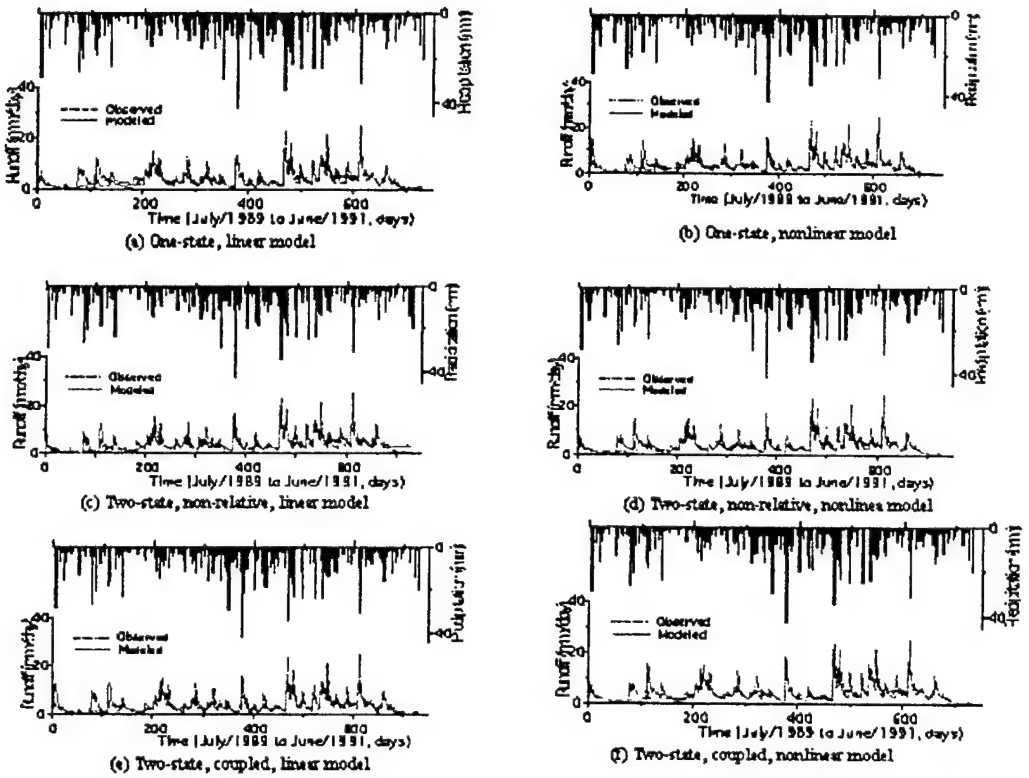

Figure 13. Forecast for the Upper West Branch, Susquehanna River using all 6 models and the observed precipitation and temperature record.

Accuracy Analysis

In order to evaluate the accuracy of each model, we used several forecast accuracy measures [Maidment,1993], to estimate forecast error. The measures include (1) mean absolute error (MAE), (2) Relative mean absolute error (RMAE), and (3) mean square error (MSE) [Baidment,1993], which are defined by

$$MAE = \frac{1}{N}\sum_{i=1}^{N}\left|q_m(i) - q_o(i)\right|$$

$$RMAE = \frac{N}{\sum_{i=1}^{N} q_o(i)}\, MAE \qquad (34)$$

$$MSE = \frac{1}{N}\sum_{i=1}^{N}\left[q_m(i) - q_o(i)\right]^2$$

The lower these measures are, the higher the prediction accuracy is. Table 3 lists the estimations of the forecast accuracy analysis for the identified models.

Model	MAE	RMAE	MSE
One-state linear system	1.214	0.3904	3.9356
Two-state uncoupled linear system	1.2917	0.4154	4.3229
Two-state coupled linear system	1.1578	0.3724	3.541
One-state nonlinear system	1.046	0.3364	3.3625
Two-state uncoupled nonlinear system	1.0295	0.3311	3.1952
Two-state coupled nonlinear system .	0.9764	0.3140	2.7560

Table 3. Forecast accuracy for the six developed models of the Upper West Branch.

We note that the two-state coupled nonlinear version of the model represents the best model performance of the Upper West Branch.

Figure 12 and 13 also show that during periods of drought as in July, August, September and October in both 1985 and 1989, the model over-estimates the runoff. We propose that a major reason for this overestimation is that unsaturated groundwater flow is not included in the initial models. In the periods of drought, the soil moisture reservoir may totally dominate the runoff by reducing recharge to saturated groundwater and absorbing all precipitation events. When rainfall occurs, the soil moisture first has to meet the deficit and satisfy soil field capacity before infiltration and recharge can occur. Future improvements to the model will explore this process.

References

Barenblatt, G.I., Iu.P. Zheltov, and I.N. Kochina, Basic concepts in the theory of seepage of homogeneous liquids in fissured rocks (strata), Prikl. Mat. Mekh., 24(5), 852-864, 1960.

Beven, K.J., Hillslope hydrographs by the finite element method, Earth Surf. Proc., 2, 13-28, 1977.

Beven, Keith, Changing ideas in hydrology-the case of physically-based models, J. Hydrol., 105, 157-172, 1989.

Beven, K., and P. Germann, Macropores and water flow in soils, Water Resour. Res., 18(5), 1311-1325, 1982.

Brandes, D. and C.J. Duffy, A dynamical model of macropore flow on hillslopes, Water Resources Research, submitted March 2000.

Brandes, D., C.J. Duffy and J.P. Cusumano, 1998 Instability and Self-Excited Oscillations in a Two-State-Variable Dynamical Model of Hillslope Soil Moisture, *Water Resources Research*, 34(12), 3303-3313.

Brooks, R.H., and A.T. Corey, Hydraulic properties of porous media, Hydrol. Paper no. 3, Civil Eng. Dept., Colorado State Univ., 1964.

Chen C., and R.J. Wagenet, Simulation of water and chemicals in macropore soils part 1. Representation of the equivalent macropore influence and its effect on soilwater flow, J. Hydrol., 130, 105-126, 1992.

Duffy, C. J., D. H. Lee and M. Jin, Dynamics of soil moisture, subsurface flow and runoff in complex terrain, 95 pp., Environ. Resour. Res. Inst., Penn. State Univ., University Park, 1994.

Duffy, C.J., A two-state integral-balance model for soil moisture and groundwater dynamics in complex terrain, Water Resour. Res., 32(8), 2421-2434, 1996.

Duffy, C. J., A, A low-dimensional model for concentration-discharge in groundwater-stream systems, 1997.

Elrick, D.E., W.D. Reynolds, H.R. Geering, and K.A. Tan, Estimating steady infiltration rate times for infiltrometers and permeameters, Water Resour. Res., 26(4), 759-769, 1990.

Freeze, R.A., Role of subsurface flow in generating surface runoff 2. Upstream source areas, Water Resour. Res., 8(5), 1272-1283, 1972.

Harlow, G.E., Jr., and LeCain, G. D., Hydraulic characteristics of, and grounwater flow, coal-bearing rocks of south western Virginia: U. S. Geological Survey Water-Supply Paper 2388, 1993.

Holland, J. H., Adaptation in natural and artificial systems, A Bradford Book, The MIT Press, Cambridge, MA, 1992.

Hursh, C.R., Storm-water and absorption, Am. Geophys. Union Trans., 17, 301-302., 1936.

Hursh, C.R, Appendix B-Report of sub-committee of subsurface-flow, Trans., Am. Geophys. Union, 25, 743-746, 1944.

Jakeman A. J. and G. M. Hornberger, How much complexity is warranted in a rainfall-runoff model, Water Resour. Res., 29(8), 2637-2649, 1993

Lynch, J. A., Effects of antecedent soil moisture on storm hydrographs, Ph.D. thesis, 41 pp., Penn. State Univ., University Park, 1976.

Lee, D. H., On nonlinear dynamics of storage-flux relationships on a hillslope, Ph.D. dissertation, 120 pp., Penn. State Univ., University Park, 1993.

Maidment, David R., Handbook of hydrology, New York, McGraw-Hill, 1993.
Crawford, N. H., and R. K. Linsley Jr., Digital simulation in hydrology: Stanford Watershed Model IV, Tech. Rep. 39, Dept. of Civ. Eng., Stanford Univ., Stanford, Calif., 1966.

Mohanty, B.P., R.S. Bowman, J.M.H. Hendrickx, and M.T. van Genuchten, New piecewise-continuous hydraulic functions for modeling preferential flow in an intermittant-flood-irrigated field, Water Resour. Res., 33(9), 2049-2063, 1997.

Othmer, H., B. Diekkruger, and M. Kutilek, Bimodal porosity and unsaturated hydraulic conductivity, Soil Sci., 152(3), 139-150, 1991.

Peters, R.R., and E.A. Klavetter, A continuum model for water movement in an unsaturated fractured rock mass, Water Resour. Res., 24(3), 416-430,1988

Richards, L.A., Capillary conduction of liquids through porous mediums, Physics, 1, 318-333, 1931.

Seaber, Paul R., J.V. Brahana and E. F. Hollyday, Appalachian Plateaus and Valley and Ridge, Hydrogeology, The Geology of North America, Volume 0-2, edited by William Back et al., 1988

Singh, Vijay P., Elementary hydrology, Prentice Hall, Englewood Cliffs, NJ 07632, 1992.

Shun, T. and C. J. Duffy, 1998, Low Frequency Oscillations in Precipitation, Temperature and Runoff Across a West-Facing Mountain Front: A Hydrogeologic Interpretation, *Water Resources Research*, 35(1), 191-201.

Tan, K.C., Y. Li, D.J. Murray-Smith and K.C. Sharman, System identification and linearisation using genetic algorithms with simulated annealing, Genetic Algorithms in Engineering System: Innovations and Applications 12-14 September 1995, Conference Publication No. 414, IEE, 1995.

Thornthwaite, C. W., An approach toward a rational classification of climate, Geographical Review, 38, p55-94, 1948.

Troch, P.A., R.P. De Troch, and W. Brutsaert, Effective water table depth to describe initial conditions prior to storm rainfall in humid regions, Water Resour. Res., 29(2), 427-434, 1993.

van Genuchten, M.Th., A closed-form equation for predicting the hydraulic conductivity of unsaturated soils, Soil Sci. Soc. Am. J., 44, 892-898, 1980.

Watson K.M. and R.J. Luxmoore. Estimating macroporosity in a forest watershed by use of a tension infiltrometer. Soil Sci. Soc. Am. J., 50, 578-582, 1986

Wilson, G.V., and R.J. Luxmoore, Infiltration, macroporosity, and mesoporosity distributions on two forested watersheds, Soil Sci. Soc. Am. J., 52, 329-335, 1988.

Zecharias, Y.B., and W. Brutsaert, Recession characteristics of groundwater outflow and base flow from mountainous watersheds, Water Resour. Res., 24(10), 1651-1658, 1988b

Yeh, G. T. 1987. FEMWATER: A finite element model of water flow through saturated-unsaturated porous media - first revision. ORNL-5567/R1. Oak Ridge National Laboratory. Oak Ridge, Tennessee. 248 p.